Journal of Translational Medicine

RESEARCH

Open Access

Irradiation-responsive PRDM10-DT modulates the angiogenic response in human NSCLC cells in an SP1-dependent manner via the miR-663a/TGF-β1 axis

Hao Huang[1†], Ying Xu[1†], Zi Guo[1], Miaomiao Zhang[1], Wanshi Li[1], Yidan Song[2], Jing Nie[1], Wentao Hu[1*], Tom K. Hei[3*] and Guangming Zhou[1*]

Abstract

Background Photon radiation has been shown to stimulate the secretion of radioresistant factors from tumor cells, ultimately promoting tumor angiogenesis and metastasis. On the other hand, heavy-ion radiotherapy has been demonstrated to control tumor angiogenesis and metastasis levels. The molecular mechanisms responsible for the different angiogenic responses to photon and heavy-ion irradiation are not fully understood. This study aims to explore the irradiation-responsive genes related to tumor angiogenesis and reveal the regulatory effect.

Methods In order to clarify the potential regulatory mechanisms of tumor angiogenesis after X-ray or carbon ion (C-ion) irradiation, we performed RNA-sequencing (RNA-seq), as well as bioinformatics, public database analysis, Western blotting, immunohistochemistry, and immunofluorescence.

Results In this study, we identified the long intergenic noncoding RNA PRDM10 divergent transcript (PRDM10-DT), which was responsive to X-rays but not carbon ions. Mechanistically, PRDM10-DT triggers tumor angiogenesis by upregulating the TGF-β1/VEGF signaling pathway through its competitive binding to miR-663a. Additionally, the transcription factor SP1 facilitated the transcription of PRDM10-DT by binding to its promoter region. It's notable that the DNA-binding activity of SP1 was enhanced by reactive oxygen species (ROS). The knockdown of either PRDM10-DT or SP1 effectively inhibited NSCLC angiogenesis and metastasis.

Conclusion These results illustrate the proangiogenic function of the PRDM10-DT/miR-663a/TGF-β1 axis and reveal the regulatory role of ROS and SP1 in the upstream response to radiation, with differential ROS production mediating the differential angiogenesis levels after X-ray and C-ion irradiation. Our findings suggest the potential of PRDM10-DT as a nucleic acid biomarker after radiotherapy and that targeting this gene could be a therapeutic strategy to counteract angiogenesis in NSCLC radiotherapy.

Keywords X-ray, Carbon ion, PRDM10-DT, TGF-β1, Angiogenesis, SP1

[†]Hao Huang and Ying Xu have contributed equally to this work.

*Correspondence:
Wentao Hu
wthu@suda.edu.cn
Tom K. Hei
tkh1@cumc.columbia.edu
Guangming Zhou
gmzhou@suda.edu.cn
Full list of author information is available at the end of the article

Introduction

According to the most recent worldwide cancer data issued in 2024, the global burden of lung cancer in terms of incidence and mortality rates is increasing rapidly [1]. As one of the primary methods for treating tumors, radiotherapy plays a crucial role in lung cancer therapy, and this need is steadily increasing [2–4]. However, the surrounding normal tissue damage can't be avoided when radiation kills tumor cells, causing side effects such as inflammation, fibrosis, and secondary tumor incidence [5, 6]. In addition, photon radiotherapy may promote angiogenesis and metastasis by altering the tumor microenvironment [7, 8]. Hypoxia and inflammation caused by radiation may activate pro-angiogenic factors such as VEGF to enhance the invasive ability of tumor cells and promote metastasis [9–11], which severely affect patient survival and have become key obstacles to improving the efficacy of photon therapy [12].

The prevalence of proton and heavy ion radiotherapy has significantly increased both the tumor control rate and patient survival rate [13, 14]. Proton and heavy ion radiotherapy have been reported to demonstrate significantly improved efficacy and lower tumor recurrence or metastasis rates than photon radiotherapy in the treatment of various stages of NSCLC [13, 15]. Kamlah et al. reported that 6 Gy X-ray irradiation significantly increased blood vessel density, whereas carbon ion (2 Gy) irradiation had no promoting effects, indicating the therapeutic advantage of carbon ions over X-rays [16]. Furthermore, some studies have reported that carbon ions induce the downregulation of motility-associated genes [17]. This implies that carbon ion radiotherapy offers an advantage in reducing tumor angiogenesis and metastasis. Therefore, exploring the underlying mechanisms of radiation-induced angiogenesis and metastasis may provide therapeutic targets for antiangiogenic therapy.

An increasing amount of evidence suggests that long noncoding RNAs (lncRNAs) play a role in the epigenetic modulation of multiple biological processes, such as metabolism, immunity, cancer, cardiovascular illnesses, and abnormalities of the nervous system [18, 19]. Nevertheless, little information has been published about the roles that lncRNAs play in controlling the different cellular responses to different kinds of radiation.

Under conditions of oxidative stress, reactive oxygen species (ROS) are essential for controlling transcription because they activate a variety of transcription factors [20]. Extensive research has shown that ROS also participates in tumor angiogenesis, cancer cell survival, and invasion [20]. Additionally, X-rays have been reported to induce more oxidation reactions and produce more ROS than C-ions do [21, 22].

Existing antiangiogenic therapies, although effective in inhibiting the tumor vascular system, often face significant limitations such as transient efficacy, development of drug resistance, bleeding risk, and adverse effects on normal vascular function [23–25]. Under the hypoxic conditions induced by these therapies, tumors often adapt to become more invasive by utilizing alternative pro-angiogenic pathways. Therefore, there is an urgent need to find new targets and therapeutic approaches. In this work, we sought to elucidate the molecular mechanism underlying radiation-induced tumor angiogenesis and metastasis. In NSCLC cell lines, we discovered that PRDM10-DT was substantially expressed in an SP1-dependent manner after X-ray irradiation and that it was positively linked with the capacity of tumor cells to promote angiogenesis, migration, and invasion. Mechanistically, we verified that PRDM10-DT can directly bind to miR-663a, hence disrupting the ability of miR-663a to inhibit TGF-β1 expression. Collectively, these findings illustrate the critical function of the SP1/PRDM10-DT/TGF-β1 axis in radiation-induced angiogenesis and metastasis. PRDM10-DT could be used as a target for antiangiogenic therapy in conventional photon radiation and as a potential diagnostic marker for NSCLC.

Materials and methods

Cell culture

The cell lines used for the research were obtained from the American Type Culture Collection (Rockville, MD, USA). DMEM and RPMI-1640 medium (Gibco, Grand Island, NY, USA) containing 100 μg/mL streptomycin, 1% penicillin sodium, and 10% fetal bovine serum (FBS) were used for cell cultivation. The cells were cultured at 37 °C in an incubator with 5% CO_2.

Cell irradiation

The cells were seeded in a T25 flask (1×10^6), and the flasks were slightly shaken to separate the cells. The Heavy Ion Medical Accelerator in Chiba (HIMAC) at the National Institute of Radiological Science (NIRS, Japan) produced the carbon ion beam, while the X-ray beam was from an RS2000 X-ray Biological Irradiator (Rad Source Technologies, GA, USA). After 24 h, the total RNA, protein, and conditioned medium of the irradiated cells were harvested for the following experiments.

RNA sequencing and ceRNA network construction

The RNA samples from the cells were harvested 24 h after radiation and immediately frozen at −80 °C. The RNA samples were subsequently subjected to RNA sequencing by Gene Denovo Biotechnology Co., Ltd (Guangzhou, China). In the data analysis program, the

FPKMs of the genes were used for filtration. Genes with an FPKM greater than or equal to 1.0 ($p < 0.05$) were selected, and the DEGs were chosen by DEseq2 with R studio software. The DEGs with a fold change greater than 2.0 ($p < 0.05$) were selected for the following analysis. The heatmap, volcano plot, and KEGG pathway enrichment analysis were performed with R packages (ggplot2, limma, pheatmapD).

To find lncRNAs that can be a prognosis biomarker after radiotherapy, we set the filter criteria that lncRNAs with HR (Hazard ratio) over 1.0 and a p value less than 0.05 related to the unirradiated group can be considered for further analysis. The HR information of lncRNAs was acquired from the lnCAR database. Based on these criteria, we selected the lncRNA PRDM10-DT with HR = 2.387 and $p = 0.042$ for further analysis. The Hazard ratios of lncRNAs can be found in Additional file 1 Table S1.

Then we predicted the miRNAs that could bind to PRDM10-DT and TGF-β1 via the ENCORI database and calculated the minimal free energy between the candidate miRNAs and PRDM10-DT or TGF-β1 via the RNAhybrid online tool. The ceRNA network was constructed via the Cytoscape program.

Gene set enrichment analysis (GSEA)

First, we calculated Spearman correlations between PRDM10-DT and each protein-coding mRNA in our RNA-seq results via the function cor.test in R. Subsequently, we used GSEA to rank the mRNAs on the basis of their correlation coefficients. We discovered that the TGF-β signaling pathway simultaneously surfaced in the KEGG and HALLMARKER gene sets and that only 15.7% of the genes in the two overlapped. The robustness of our analysis was ensured by integrating the above two pathways into the TGF-β signaling pathway, which includes 121 genes.

Cell transfection and lentiviral transduction

The lentivirus overexpressing PRDM10-DT and the matched negative control lentivirus were provided by Shanghai Genechem Co., Ltd. RiboBio (Guangzhou, China) designed and produced all the shRNAs, miRNA mimics, and inhibitors of miRNA, as well as their corresponding negative controls. Lung cancer cells were cultured in these lentivirus-containing media for 72 h and selected with 2 μg/mL puromycin (Invitrogen). The sequences of the shRNAs and siRNAs used are listed in the Additional file 1 Table S3.

Western blotting

Beyotime (Shanghai, China) provided RIPA lysis buffer for the collection of cell lysates. The proteins were separated via SDS–PAGE and transferred to PVDF membranes via traditional methods. After incubation with primary and HRP-conjugated secondary antibodies, the chemiluminescence signal of the target protein was measured. In this study, antibodies against the following proteins were used: TGF-β1 (CST-3711, Beverly, MA, USA), SP1 (Ab231778), VEGF (19003-1-AP, Proteintech, Chicago, IL, USA), and GAPDH (CST-5174, Beverly, MA, USA). The secondary antibodies, including anti-mouse IgG (A0216) and anti-rabbit IgG (A0208), were purchased from Beyotime.

RNA reverse transcription and RT–qPCR

After total RNA extraction, the PrimeScript RT Reagent Kit (Kusatsu, Shiga, Japan) was used for lncRNA and mRNA reverse transcription. RiboBio (Guangzhou, China) supplied primers for miR-663a and U6 RT–qPCR. GAPDH and U6 were selected as the internal controls, and all the data were analyzed via the relative quantification ($2^{-\Delta\Delta CT}$) method. Additional file 1 Table S3 lists the primer sets used.

Tube formation assays

A549 and H1299 cells were preseeded in 60 mm dishes. When the cell density reached 60–70%, C-ion or X-ray irradiation was administered. The conditioned medium taken from the irradiated cells was used for the tube formation assay, and PeproTech (Rocky Hill, NJ, USA) provided the recombinant human TGF-β1 protein for cell treatment. Precooled Matrigel (Corning, New York, NY, USA) was plated in 96-well plates at 50 μL/well and incubated at 37 °C to solidify for 30 min. Then, the human umbilical vein endothelial cells (HUVECs) were digested and collected by centrifugation (1000 rpm, 5 min), resuspended in the above collected conditional media, and seeded in 96-well plates at 2×10^4/well. Images of the HUVEC tubes were taken with a Leica inverted phase-contrast microscope (Leica, Wetzlar, Germany) at different time points and analyzed with the Angiogenesis Analyzer plugin for ImageJ.

Wound healing assays

Cells were seeded in six-well plates and cultivated to 90% confluence. Next, we created wounds with monolayer cells via a 200 μL pipette tip. Wound images captured

by a microscope were analyzed via ImageJ software. The ratio of the decreased wound area at 24 h to 0 h in each group was calculated to indicate the cell migration ability.

Transwell assays

To test the invasive ability of the cells, 24-well plates containing transwell chambers (NEST, China) were used. First, 60 μL of Matrigel (Corning, USA) was added to the upper chamber, and the plates were subsequently incubated in a 37 °C incubator to solidify for 30 min. The lower chamber was then immersed in FBS-containing media, and the top chamber was filled with 5×10^4 cells suspended in 200 μL of culture medium (without FBS). After 36 h of incubation, we carefully removed the remaining cells in the upper chamber. The invasive cells were then fixed in the lower chamber with 75% ethanol for 15 min, followed by 0.1% crystal violet staining. Finally, an inverted phase contrast microscope was used to obtain images of five random fields of view for subsequent invasive cell counting.

Dual-luciferase reporter assay

The ENCORI online database predicted the potential binding sites of miR-663a with PRDM10-DT and the TGF-β1 3′UTR. The pmiR-RB-reporter dual-luciferase vectors containing wild-type and mutant sequences of target genes were obtained from RiboBio (Guangzhou, China). These vectors were named PRDM10-DT-WT, PRDM10-DT-Mut, TGF-β1-WT, and TGF-β1-Mut, respectively, and were cotransfected with miR-663a mimics or miR-NC into cells together. We used the Dual-Luciferase Reporter Gene Assay Kit (Beyotime, Shanghai, China) to measure the luciferase activity of the transfected cells according to the manufacturer's instructions.

RNA fluorescence in situ hybridization (FISH)

Following the manufacturer's instructions, a FISH assay was performed to determine the subcellular localization of PRDM10-DT in lung cancer cells. The Cy3-labeled PRDM10-DT probes and Fluorescent In Situ Hybridization Kit were provided by RiboBio (Guangzhou, China). Photographs of the cells were then captured via an Olympus laser scanning confocal microscope.

RNA immunoprecipitation (RIP)

RiboBio (Guangzhou, China) synthesized the biotin-labeled PRDM10-DT probe, miR-663a mimics, and miR-NC. First, we transfected cells with either miR-NC or miR-663a mimics. Next, we fixed the cells for 10 min with 1% formaldehyde and lysed them with radioimmunoprecipitation assay (RIPA) buffer (Beyotime, Shanghai, China). Then, the lysate was sonicated and centrifuged to obtain the supernatant, and 50 μL of the supernatant was removed as input. Next, we added PRDM10-DT-specific probe-streptavidin Dynabeads (M-280, Invitrogen) to the remaining part of the supernatant and incubated the mixture at 30 °C for more than 12 h. After that, 200 μL of lysis buffer containing proteinase K was added to the washed lncRNA-probe-dynabead mixture. Eventually, the RNA in the mixture was isolated by using Invitrogen TRIzol reagent (CA, USA), and RT–qPCR analysis was performed.

Enzyme-linked immunosorbent assay (ELISA)

The TGF-β1 and VEGF protein contents of the serum samples or cell supernatants were quantified via the Human/Mouse/Rat TGF-β1 ELISA Kit (Multi Sciences, Hangzhou, China), Mouse VEGF ELISA Kit (Multi Sciences, Hangzhou, China), and Human VEGF ELISA Kit (Multi Sciences, Hangzhou) according to the manufacturer's instructions. The use of human serum samples from 8 non-small cell lung cancer patients who had received radiotherapy. Four patients received C-ion radiotherapy (67.5 ± 5.0 Gy, 20 ± 0.0 Fractions), and the other four received X-ray radiotherapy (67.5 ± 3.0 Gy, 33.8 ± 1.5 Fractions). Patients' demographic and clinical characteristics can be found in Additional file 1 Table S2.

Nude mouse tumorigenesis and treatment

Shanghai SLAC Laboratory Animal Co., Ltd., provided 6–8-week-old male BALB/c nude mice for the animal experiments. Animal rooms with a specific pathogen-free (SPF) environment were used to raise these mice. The protocols for the animal experiments were examined and approved by the Institutional Animal Care and Use Committee of Soochow University. For the mouse subcutaneous tumor model, the right flank of each mouse was injected with 5×10^6 A549 cells that were suspended in 100 μL of PBS. When the tumor volume reached approximately 100 mm^3, the mice were given 5 Gy X-rays to target the tumor, and lead sheets were used to protect the remaining parts of their bodies. All of the mice were divided into five groups: si-NC, IR, IR + si-NC, IR + si-PRDM10-DT, and IR + si-SP1. On the fifth day after irradiation, each mouse was intratumorally injected with si-NC (0.625 nmol, 25 μL), si-PRDM10-DT (0.625 nmol, 25 μL), or si-SP1 (0.625 nmol, 25 μL) according to the grouping situation. Moreover, beginning on the 20th day, the mice were given intratumoral injections once every 5 days until all eight rounds of injections were finished

on the 55th day. Every 5 days, the body weight and tumor volume of each mouse were recorded. All of the animals were sacrificed on day 56 to harvest their tumors and serum. The sequences of the siRNAs used in the animal experiments can be found in the Additional file 1 Table S3.

Lentivirus containing either sh-PRDM10-DT or sh-NC sequences was used to transduct A549 cells. Following puromycin selection (2 μg/mL), stable cells (5×10^6 cells per mouse) were injected into nude mice through tail vein injection. Metastatic progression was monitored 2 weeks post-injection by measuring luciferase intensity using an IVIS imaging system.

Hematoxylin & eosin (H&E) staining and immunohistochemistry (IHC)

The tissues were preserved with formalin and embedded in paraffin, after which the embedded tissues were processed into sections. Hematoxylin and eosin (HE) staining was performed with a hematoxylin–eosin (HE) staining kit (Solarbio, Beijing, China). Using a standard methodology, immunohistochemical (IHC) staining was applied to the subcutaneous tumor slices. The primary antibodies used were CD31 (CST-77699), VEGF (Proteintech, 19003–1-AP), TGF-β1 (CST-3711), SP1 (Abcam, ab231778), and Ki-67 (CST, 9449). The sections were incubated with secondary antibodies (PV-6001, PV-6002, ZSGB-BIO, Beijing, China) at 37 °C for 30 min. Finally, DAB color rendering, dehydration, and neutral balsam sealing were performed, and the slides were scanned with the DMS-10 Digital Pathological Section Scanner System (Dmetrix, Suzhou, China) to acquire high-quality images. The positive rate of the target protein in the tissues was analyzed via the ImageJ plugin IHC-profiler.

Statistical analysis

The group differences in the Kaplan–Meier survival curves were determined via the log-rank test. Student's *t* test was used to examine the differences between the experimental and control groups. Each experiment was run at least three times, and the data are shown as the mean ± standard deviation (SD). For the statistical analyses, two-tailed *p* values were used, and a *p* value of less than 0.05 was considered statistically significant.

The effect size calculation was based on Cohen's d formulae: Cohen's $d=(x1-x2)/\text{pooled SD}$. The statistical power analyses were performed with R-studio software and the "pwr" R package according to Cohen's d, sample size, and sig. level of each group. The results of Cohen's d and statistical power can be found in Additional file 1 Table S6.

Results

X-rays stimulate the upregulation of PRDM10-DT in NSCLC cells and lung metastases in vivo

First, A549 cells expressing luciferase were irradiated with X-ray (2 Gy) or C-ion (2 Gy) and subsequently injected into nude mice through the tail vein. After 3 weeks, the luciferase activity of the cancer nodules was tested via the IVIS system. In vivo experiments revealed that A549 cells in the X-ray-treated group formed more metastases than those in the C-ion group did (Fig. 1A, B). The HE staining results also suggested greater nodule formation in the X-ray group than in the C-ion group (Fig. 1C). Additionally, although the difference was not statistically significant, we observed an increasing trend in the number of metastatic sites in the X-ray group relative to the control group.

To screen for genes that might react to X-ray or C-ion irradiation in lung cancer cells, A549 cells were irradiated by X-ray or C-ion in vitro, and followed with RNA-seq. The differentially expressed genes were then filtered and analyzed via R language. For upregulated lncRNAs responsive to X-rays, we conducted hazard ratio (HR) evaluation via the online database lnCAR (https://lncar.renlab.org). Among the 46 lncRNAs upregulated by X-rays (Fig. 1D, E), PRDM10-DT was the only lncRNA with an $HR>1.0$ and $p<0.05$ (Table S1). However, PRDM10-DT is not involved in the differential expression of lncRNAs responsive to C-ion irradiation (Fig. 1D, E). Based on TCGA data analysis, there was a considerable increase in PRDM10-DT expression in lung tumor tissues compared with matched normal peritumoral tissues (Fig. 1F). Moreover, there was a negative correlation between PRDM10-DT expression and the overall survival (OS) rate of patients with lung cancer, suggesting that PRDM10-DT may function as an oncogene (Fig. 1G).

Differential expression of PRDM10-DT after X-ray and carbon ion irradiation reflects the complexity of tumor cell response mechanism to different types of radiation. X-rays induce cell damage through indirect effects such as free radical generation, which may activate DNA damage repair pathways and a series of radiation-responsive gene expressions. Thus, indirect upregulation of PRDM10-DT is a kind of resistant reaction of tumor cells under radiation. In other words, X-rays caused more sub-lethal injury than C-ion, thus the tumor cells have more chance to activate damage repair reactions to survive, thereby reducing the killing effect of radiotherapy. In contrast, C-ion irradiation usually causes lethal injury and triggers apoptosis and necrosis pathways directly without activating the protective regulation of oncogenes, which was manifested as the low responsiveness of PRDM10-DT expression.

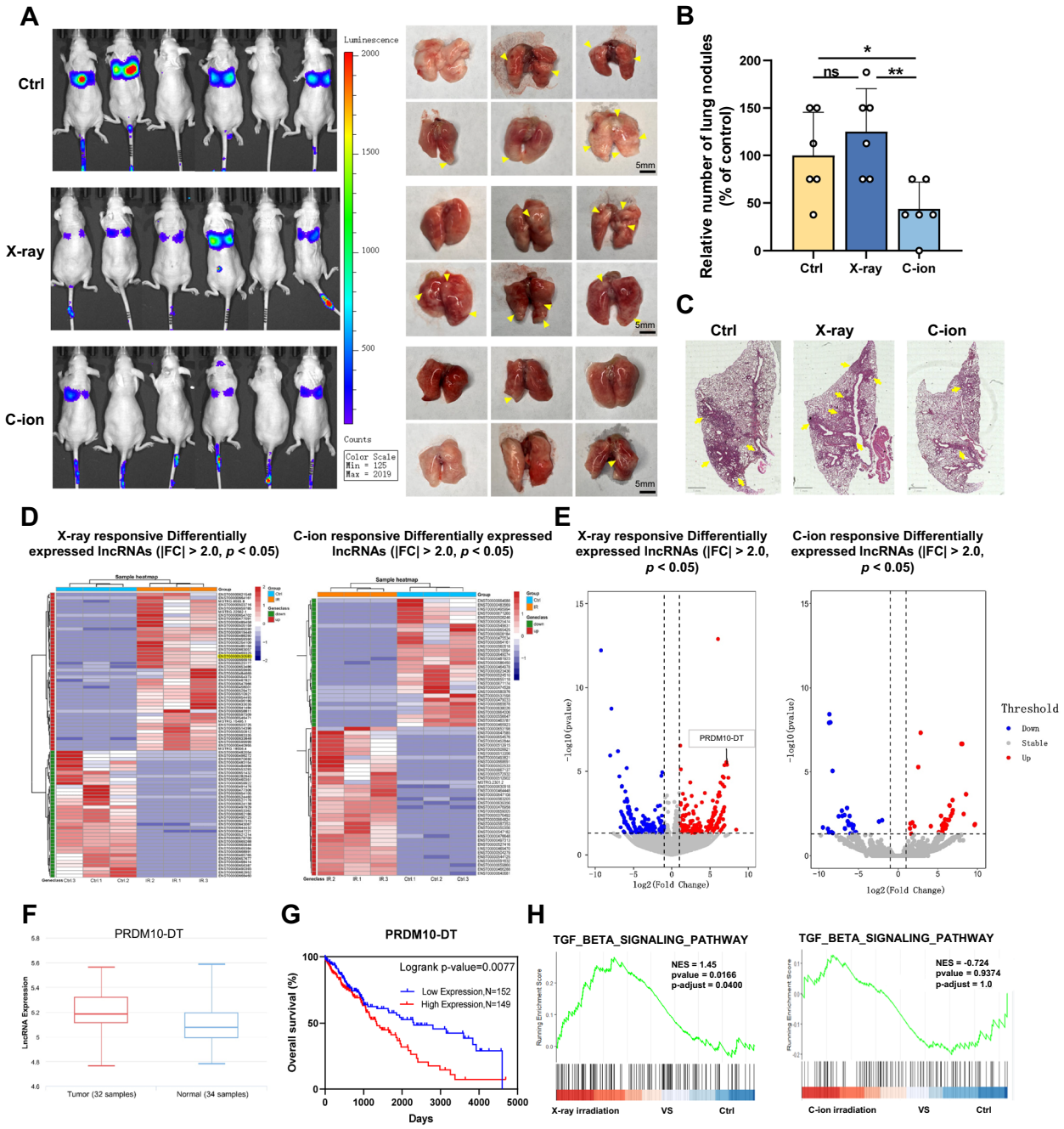

Fig. 1 PRDM10-DT is a prognostic risk factor for X-ray-induced lung metastasis. **A** 2 Gy X-ray- or C-ion-irradiated NSCLC tumor cells were injected intravenously into the mice, and the luciferase intensity at the metastasis sites was checked via an IVIS imaging system after 3 weeks. The lung tissues were isolated and photographed and then processed into sections for metastasis site determination. $n = 6$. **B**,**C** Quantification of metastasis sites and HE-stained images of lung tissues. $n = 6$. **D** Heatmap showing the differentially expressed lncRNAs in X-ray- or C-ion-irradiated NSCLC samples ($p < 0.05$, FC > 2.0). **E** Volcano plot displaying the significantly upregulated or downregulated lncRNAs described in **D** after irradiation. The blue and red dots indicate significantly changed genes ($p < 0.05$, FC > 2.0). **F** The lncCAR online database provides the PRDM10-DT expression levels in NSCLC tumor and normal tissues. **G** The survival curves of NSCLC patients with different expression levels of PRDM10-DT were retrieved from the OncoLnc database. **H** GSEA results showing the enrichment of the differentially expressed mRNAs affected by PRDM10-DT in the TGF-β signaling pathway after X-ray or C-ion irradiation. The data are presented as the means ± standard deviations (SDs). ^{ns} $p > 0.05$; * $p < 0.05$; ** $p < 0.01$

The KEGG pathway enrichment analysis results for radiation-responsive mRNAs indicated that the TGF-β1 signaling pathway was significantly upregulated in X-ray-irradiated cells, but not in C-ion-irradiated cells (Additional file 1 Fig. S1E, F). Furthermore, we performed GSEA for the differentially expressed mRNAs that were likely influenced by PRDM10-DT post-radiation. The results show that PRDM10-DT-influenced mRNAs in X-ray group obviously enriched in TGF-β signaling pathway (NES = 1.45, $p = 0.0166$) but not in C-ion group (NES = −0.724, $p = 0.9374$) (Fig. 1H). These data suggest that PRDM10-DT may be related to the activation of the TGF-β pathway and NSCLC metastasis during X-ray irradiation, which differs from in C-ion irradiation.

X-rays cause greater release of proangiogenic factors than C-ions do in NSCLC cells

Angiogenesis is required for tumor growth and dissemination. Many studies have reported that X-ray irradiation promotes tumor angiogenesis and metastasis, in addition to its ability to kill tumor cells [26]. However, patients who receive carbon ion radiotherapy reportedly have relatively lower levels of angiogenesis and metastasis than those who receive X-rays [27, 28]. In this study, the IHC staining and quantification data revealed that X-ray exposure led to significant upregulation of VEGF, TGF-β1, and CD31 proteins, whereas the C-ion group presented significantly lower level of these three proteins compared to X-ray group ($p < 0.01$) (Fig. 2A, D). These data confirm that lung cancer cells irradiated with X-rays exhibit greater proangiogenic factor expression than do cells irradiated with C-ions in vivo.

Subsequently, we collected conditioned media (CMs) from A549 cells that had been exposed to either C-ion or X-ray radiation. These CMs were then incubated with HUVECs, after which a tube formation assay was performed to assess their proangiogenic ability. The results suggest that CM from X-ray-irradiated cells induced greater HUVEC tubulogenesis degree than CM from C-ion-irradiated cells (Fig. 2E, F). Consistently, X-rays irradiation induced greater PRDM10-DT, TGF-β1, and VEGF expression than C-ions did in A549 cells (Fig. 2G, H). Furthermore, we evaluated the serum levels of TGF-β1 and VEGF in patients undergoing radiotherapy. Compared with those who received C-ion radiotherapy, patients who underwent X-ray radiotherapy presented elevated serum levels of TGF-β1 and VEGF ($p < 0.05$) (Fig. 2I; Table S2). In addition, through analysis of survival data from an online database (OncoLnc), we found that patients with higher TGF-β1 and VEGF levels had poorer prognoses ($p < 0.05$) (Fig. 2J). The above data suggest that X-rays can induce greater levels of angiogenesis and can enhance PRDM10-DT, TGF-β1, and VEGF expressions than C-ions.

PRDM10-DT enhances angiogenesis and metastasis in NSCLC cells

To verify the proangiogenic and prometastatic abilities of PRDM10-DT in vitro, we constructed a PRDM10-DT-overexpressing lentivirus (LV-PRDM10-DT) and a negative control lentiviral vector (LV-NC). A549 and H1299 cells were operated with lentiviral transduction to establish the PRDM10-DT overexpression cell lines (Fig. 3A). The HUVEC tube formation assay results revealed that the upregulation of PRDM10-DT significantly enhanced the proangiogenic ability of conditioned media from A549 (A549-CM) and H1299 (H1299-CM) cell lines ($p < 0.05$) (Fig. 3B, C). Since angiogenesis is linked to tumor metastasis [29–31], we investigated whether PRDM10-DT affects the capacity for cell metastasis. The results revealed that the migration rate (Fig. 3D, E) and the number of invasive cells (Fig. 3F, G) were markedly increased in the LV-PRDM10-DT group ($p < 0.01$).

Next, we constructed shRNAs targeting PRDM10-DT (shPRDM10-DT#1 and shPRDM10-DT#2) and transfected them into A549 and H1299 cells (Fig. 3H). Twenty-four hours post transfection, the conditioned media of the cells were collected for coincubation with HUVECs, and the pro-tubulogenesis ability of A549-CM or H1299-CM was decreased by the knockdown of PRDM10-DT ($p < 0.01$) (Fig. 3I, J). Similarly, silencing of PRDM10-DT markedly impaired the cell migration rate (Fig. 3K, L) and invasion ability (Fig. 3M, N) ($p < 0.05$). These results imply that PRDM10-DT may play a role in controlling angiogenesis and lung cancer cell dissemination.

PRDM10-DT controls the production of TGF-β1/VEGF by sponging miR-663a

It has been demonstrated that TGF-β1 and VEGF are crucial for angiogenesis [32, 33]. According to previous RNA-seq analysis, TGF-β1 was found to be activated by X-ray irradiation but not by C-ion beams. As shown in Fig. 4A and B, the overexpression of PRDM10-DT (LV-PRDM10-DT) induced the upregulation of TGF-β1 and VEGF at both the transcriptional and translational levels ($p < 0.05$). In addition, TGF-β1 (1 ng/mL) treatment indcued a notable upregulation of VEGF expression ($p < 0.05$). In contrast, the upregulation of TGF-β1 and VEGF induced by X-ray irradiation can be rescued by the knockdown of PRDM10-DT, which was similar to the findings in the TGF-β1 inhibitor treatment group ($p < 0.05$) (Fig. 4C, D).

Next, we predicted the localization of PRDM10-DT in A549 and H1299 cells via an online tool (lncLoactor)

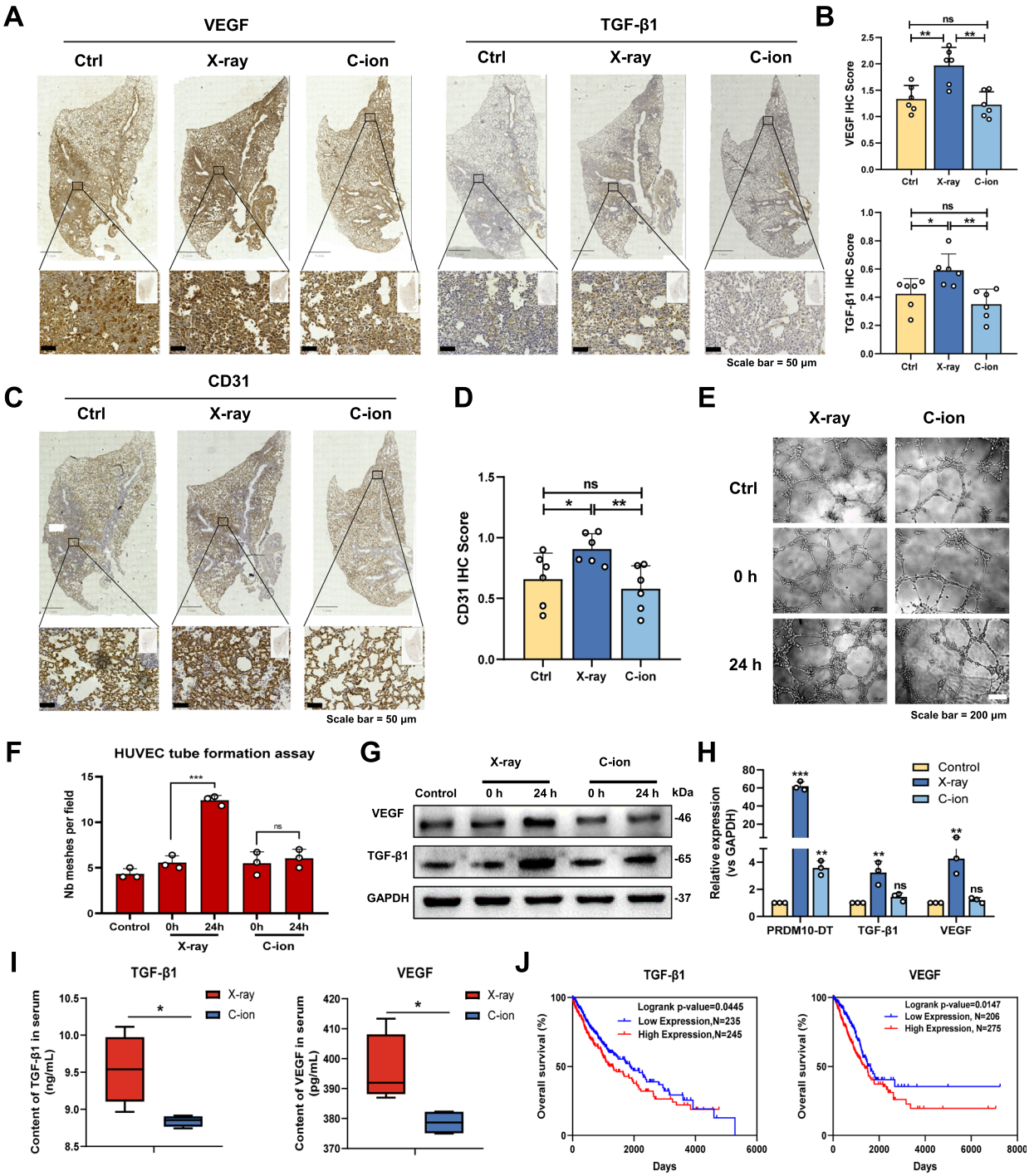

Fig. 2 X-rays induce greater angiogenesis than C-ions do in NSCLC cells. **A** X-ray (2 Gy)- or C-ion (2 Gy)-irradiated NSCLC tumor cells were injected intravenously into mice, and IHC staining of the VEGF and TGF-β1 proteins was performed. $n = 6$. **B** The IHC scores of VEGF and TGF-β1 in **A** were analyzed via ImageJ software. $n = 6$. **C**,**D** CD31 staining and IHC scoring were performed on mouse lung tissues. $n = 6$. **E**,**F** CM from irradiated A549 cells was collected and used for the HUVEC tube formation assay. $n = 3$. **G** TGF-β1 and VEGF protein levels in A549 cells were measured after irradiation. **H** Relative transcription of PRDM10-DT, TGF-β1, and VEGF in A549 cells following X-ray or C-ion irradiation. $n = 3$. **I** The TGF-β1 and VEGF protein levels in the serum of patients who underwent X-ray or C-ion radiotherapy were assessed via ELISA. $n = 4$. **J** The correlation between the overall survival rate of NSCLC patients and the expression of TGF-β1 or VEGF was obtained from the OncoLnc database. The data are presented as the means ± standard deviations (SDs). ^{ns} $p > 0.05$; * $p < 0.05$; ** $p < 0.01$; and *** $p < 0.001$

and confirmed its subcellular distribution via FISH (Fig. 4E, F). The results demonstrated that PRDM10-DT was found in both the cytoplasm and the nucleus, with a greater concentration in the latter (Fig. 4G). Furthermore, we explored the potential ceRNA regulatory mechanism and identified several microRNAs that can form a ceRNA network with PRDM10-DT and TGF-β1 mRNAs. First, we identified 7 candidate miRNAs that can target both PRDM10-DT and TGF-β1 based on the ENCORI online database, and constructed lncRNA-miRNA-mRNA regulatory network (Fig. 4H, I). Next, we utilized the RNAhybrid online tool to compute the minimal free energy (Mfe) between the candidate miRNAs and the PRDM10-DT or TGF-β1 mRNAs. The results suggested that miR-663a has the lowest Mfe with PRDM10-DT and TGF-β1, indicating that miR-663a has the most stable connection with these two targets (Fig. 4J).

In a subsequent study, miR-663a downregulation was found to augment TGF-β1 and VEGF production and enhance the proangiogenic, migratory, and invasive characteristics of A549 and H1299 cells. Conversely, the upregulation of miR-663a had the opposite effect (Additional file 1 Figs. S1E, F, S3, S4). These data suggest that PRDM10-DT can facilitate tumor angiogenesis through the TGF-β1/VEGF axis, possibly by suppressing miR-663a.

ROS-activated SP1 triggers the transcription of PRDM10-DT

In the above research, we confirmed the proangiogenic and prometastatic functions of the PRDM10-DT/miR-663a/TGF-β1 axis in NSCLC, as well as its involvement in X-ray-induced tumor angiogenesis and metastasis. But how X-rays induce up-regulation of PRDM10-DT are still unclear. According to some published studies, X-rays produce more ROS than iso-dose C-ions do, thus leading to different biological effects [22, 34]. Additionally, it has been shown that ROS activates various transcription factors such as AP1, Nrf2, and p53 that control a wide range of biological activities [20, 35, 36]. Thus, we hypothesized that the ROS produced by irradiation induces certain ROS-responsive transcription factors (TFs) to bind to the PRDM10-DT promoter region and activate the corresponding transcription program. Then we confirmed that ROS production induced by 2 Gy X-rays was significantly greater than that induced by 2 Gy C-ions ($p < 0.05$) (Fig. 5A), which is consistent with published research. Next, we screened potential TFs that can bind to the PRDM10-DT promoter region via the UCSC, hTFtarget, and AnimalTFDBv4.0 databases and then intersected the results with known human TFs. Finally, 21 TFs were screened and ranked according to their JASPAR binding scores (Fig. 5B). Through silencing the top 10 TFs, we revealed that the knockdown of RREB1, YY1, and SP1 decreased PRDM10-DT expression after X-ray irradiation ($p < 0.01$) (Fig. 5C). Then, a luciferase reporter assay revealed that only SP1 is responsive to both IR and H_2O_2 treatment, resulting in increased binding to the PRDM10-DT promoter region ($p < 0.05$) (Fig. 5D).

Additionally, the results of the ChIP experiment confirmed that the binding of SP1 to the PRDM10-DT promoter is ROS dependent (Fig. 5E). The si-SP1 and SP1 inhibitor mithramycin (200 nM) treatment decreased the transcript levels of PRDM10-DT, TGF-β1, and VEGF in A549 and H1299 cells ($p < 0.05$) (Fig. 5F). Similarly, the protein levels of TGF-β1 and VEGF were also reduced in the si-SP1 and mithramycin groups ($p < 0.05$) (Fig. 5G). Further investigation suggested that the inhibition of SP1 decreased the pro-angiogenesis ability of the CMs from A549 and H1299 cells ($p < 0.05$) (Fig. S5A, B). Functionally, the invasion and migration ability of cells were dramatically reduced by SP1 suppression ($p < 0.01$) (Fig. S5C, F). These data suggest that ROS induces SP1 binding to the PRDM10-DT promoter region after irradiation, thereby promoting the transcription of PRDM10-DT.

PRDM10-DT and SP1 are potential antiangiogenic targets for NSCLC radiotherapy

We constructed A549 subcutaneous tumor model, the tumor sites were exposed to 5 Gy X-ray radiation and

(See figure on next page.)

Fig. 3 Upregulation of PRDM10-DT promotes angiogenesis and metastasis in NSCLC cells in vitro. **A** Cells were performed lentiviral transduction with negative control lentivirus (LV-NC) or PRDM10-DT-overexpressing lentivirus (LV-PRDM10-DT) and then subjected to RT–qPCR to assess the expression of PRDM10-DT. **B** A HUVEC tube formation assay was used to assess the proangiogenic potential of CM from LV-NC or LV-PRDM10-DT cells. Scale bar = 200 μm. **C** The number of meshes per field in **B**. **D** A wound healing assay was conducted to evaluate the migration ability of cells. Scale bar = 200 μm. **E** The relative migration rate of the two cell lines in **D** was analyzed. **F** Transwell assays were used to detect invasive ability. Scale bar = 200 μm. **G** The number of invasive cells in **F** was counted. **H** A549 and H1299 cells were transfected with shRNAs (shNC, shPRDM10-DT#1, shPRDM10-DT#2) and then subjected to RT–qPCR to assess the expression of PRDM10-DT. **I**,**J** The conditioned medium of the cells in **H** was collected for the HUVEC tube formation assay. Scale bar = 200 μm. **K**,**L** The migration ability of the cells in **H** was tested via a wound healing assay, and the relative migration rate of the cells was quantified. Scale bar = 200 μm. **M**,**N** The invasive ability of the cells in **H** was tested, and the number of invasive cells was quantified. Scale bar = 200 μm. The data are presented as the means ± standard deviations (SDs) and $n = 3$. * $p < 0.05$; ** $p < 0.01$; and *** $p < 0.001$

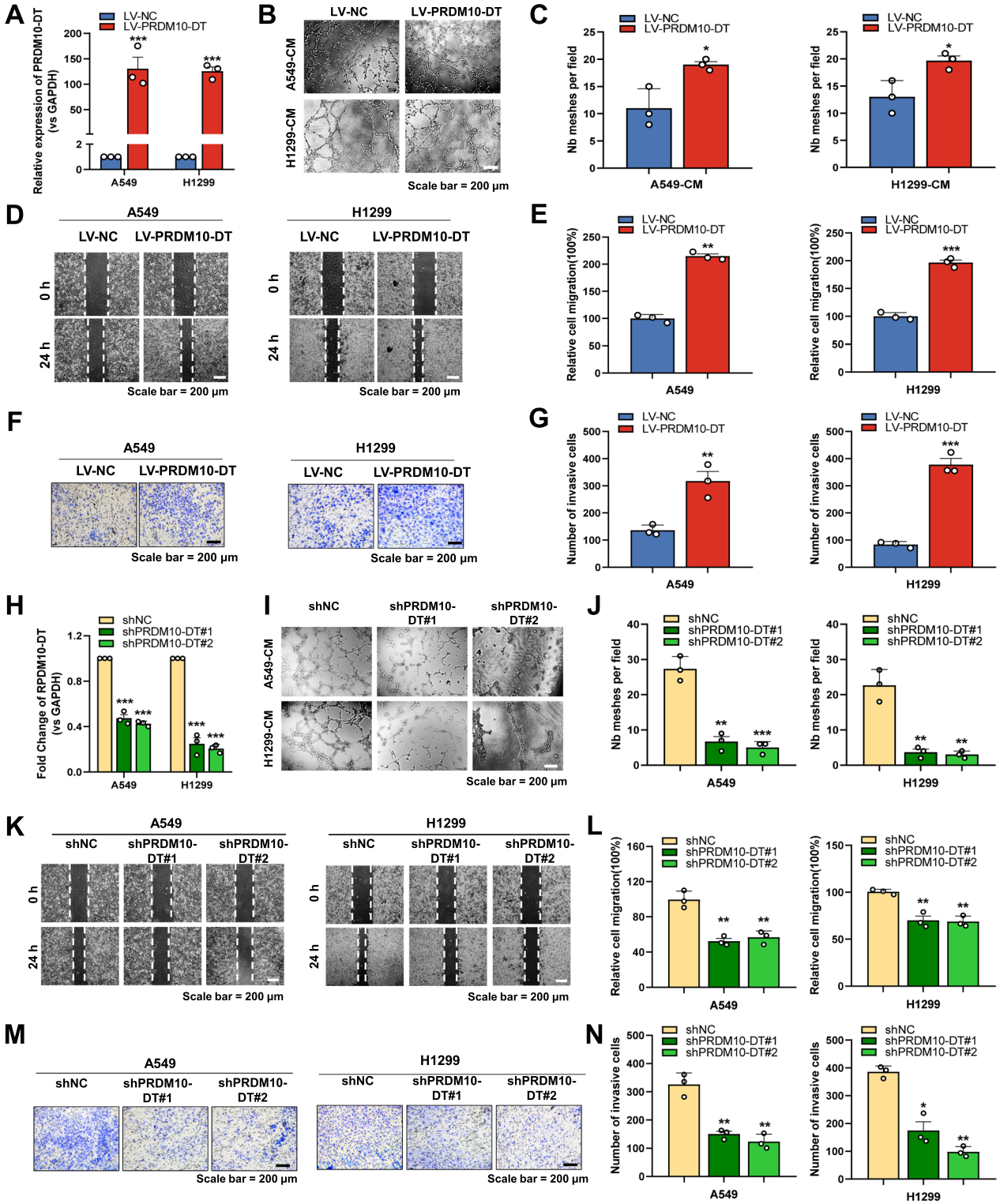

Fig. 3 (See legend on previous page.)

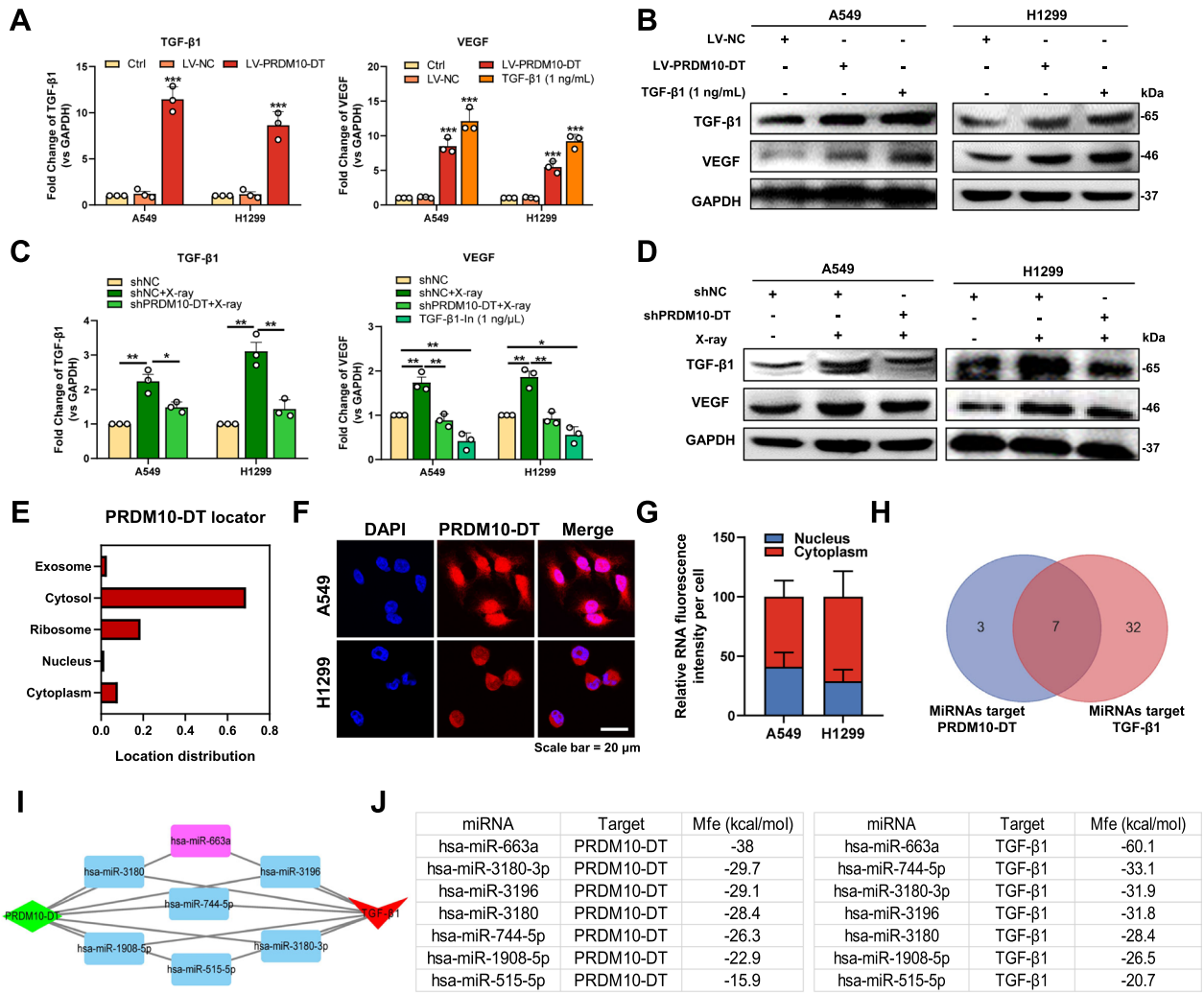

miRNA	Target	Mfe (kcal/mol)
hsa-miR-663a	PRDM10-DT	-38
hsa-miR-3180-3p	PRDM10-DT	-29.7
hsa-miR-3196	PRDM10-DT	-29.1
hsa-miR-3180	PRDM10-DT	-28.4
hsa-miR-744-5p	PRDM10-DT	-26.3
hsa-miR-1908-5p	PRDM10-DT	-22.9
hsa-miR-515-5p	PRDM10-DT	-15.9

miRNA	Target	Mfe (kcal/mol)
hsa-miR-663a	TGF-β1	-60.1
hsa-miR-744-5p	TGF-β1	-33.1
hsa-miR-3180-3p	TGF-β1	-31.9
hsa-miR-3196	TGF-β1	-31.8
hsa-miR-3180	TGF-β1	-28.4
hsa-miR-1908-5p	TGF-β1	-26.5
hsa-miR-515-5p	TGF-β1	-20.7

Fig. 4 PRDM10-DT stimulates the expression of VEGF and TGF-β1 in NSCLC cells. **A** Relative mRNA expression of TGF-β1 and VEGF in lentiviral transducted A549 and H1299 cells. $n = 3$. **B** The protein levels of TGF-β1 and VEGF in lentiviral transducted lung cancer cells. $n = 3$. **C** Following transfection with shNC or shPRDM10-DT, A549 and H1299 cells were subjected to 2 Gy X-ray radiation. Twenty-four hours after irradiation, the relative mRNA levels of TGF-β1 and VEGF were tested via RT–qPCR. $n = 3$. **D** The protein levels of TGF-β1 and VEGF in the A549 and H1299 cells in **C** were tested by Western blotting. $n = 3$. **E** The PRDM10-DT subcellular distribution was predicted by lncLoactor. **F** Localization of PRDM10-DT in A549 and H1299 cells. Nuclei were stained with DAPI (blue), and PRDM10-DT was labeled with Cy3-labeled PRDM10-DT-specific probes (red). Scale bar = 20 μm. **G** Quantification of the PRDM10-DT subcellular distribution ratio in the nucleus or cytoplasm. **H** The miRNAs that could target PRDM10-DT and TGF-β1 were predicted via the ENCORI database. **I** The PRDM10-DT-miRNA-TGF-β1 ceRNA network was constructed via Cytoscape. **J** The Mfe between miRNAs and their target genes. The data are presented as the means ± standard deviations (SDs). * $p < 0.05$; ** $p < 0.01$; and *** $p < 0.001$

administered PRDM10-DT silencing (si-PRDM10-DT) or SP1 silencing (si-SP1) treatment through intratumor injections every 5 days (Fig. 6A). The si-PRDM10-DT and si-SP1 treatments markedly delayed tumor growth ($p < 0.05$) without causing significant body weights change during the 40-day treatment period, indicating the safety of this therapy on the whole body (Fig. 6B–D; Fig. S6). Moreover, mouse serum TGF-β1 and VEGF protein levels were increased by irradiation, but inhibited by downregulation of PRDM10-DT and SP1 notably ($p < 0.05$) (Fig. 6E).

In dissected tumor tissues shown in Fig. 6F, we confirmed the upregulation of angiogenesis markers such as TGF-β1, VEGF, and CD31 in the IR group, as well as the downregulation of them in the si-PRDM10-DT and si-SP1group ($p < 0.01$). In H&E-stained sections, the reduced microvessel density (MVD) in si-PRDM10-DT or si-SP1 group indicated the anti-angiogenic effect

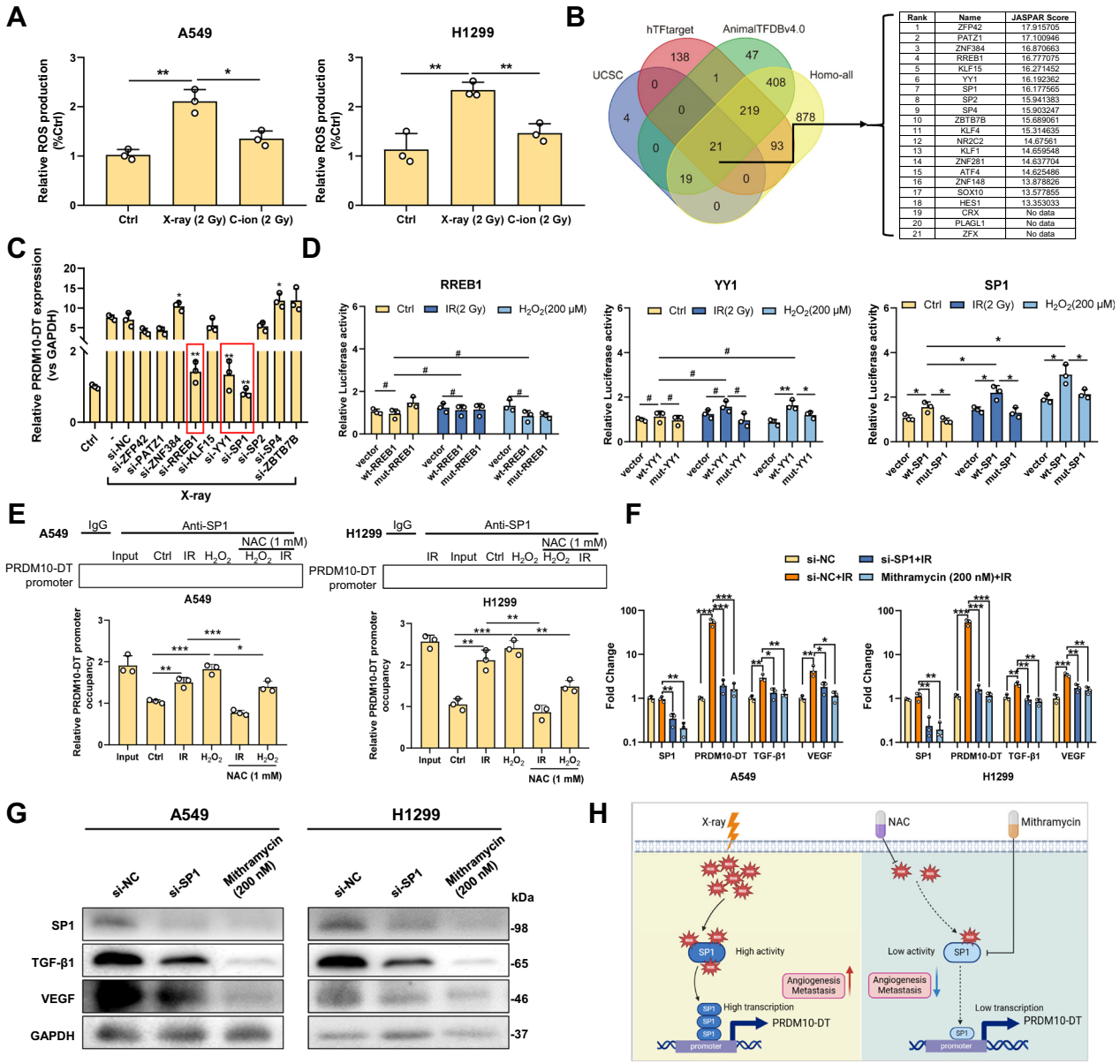

Fig. 5 X-ray irradiation promotes the SP1-mediated transcription of PRDM10-DT in a ROS-dependent manner. **A** ROS levels in X-ray- or C-ion-irradiated A549 and H1299 cells. $n = 3$. **B** The potential transcription factors capable of binding to the PRDM10-DT-promoter region were predicted via the UCSC, hTFtarget, and AnimalTFDBv4.0 databases, and intersections were made with all existing human (Homoall) transcription factors. The binding scores of 21 filtered TFs in the PRDM10-DT-promoter region were predicted via the JASPAR database. **C** The top 10 TFs in **B** were silenced in X-ray-irradiated A549 cells via siRNA, and the PRDM10-DT transcriptional level was subsequently measured. $n = 3$. **D** A luciferase reporter vector containing the PRDM10-DT promoter region sequence and plasmids containing RREB1, YY1, and SP1 wild-type (wt) or mutant (mut) sequences were cotransfected into A549 cells, which were subsequently subjected to 2 Gy X-ray or 200 μM H_2O_2 treatment, and the luciferase activity was measured after treatment. $n = 3$. **E** A ChIP experiment was carried out to detect the connection of SP1 in the PRDM10-DT promoter region with or without ROS. $n = 3$. **F** After si-SP1 transfection or 200 nM mithramycin treatment, A549 and H1299 cells were exposed to 2 Gy X-rays. Next, the relative transcript expression levels of VEGF, TGF-β1, PRDM10-DT, and SP1 were determined. $n = 3$. **G** The levels of the SP1, TGF-β1, and VEGF proteins in cells subjected to various treatments. $n = 3$. **H** Schematic diagram illustrating X-ray-induced PRDM10-DT transcriptional activation and the downregulation of angiogenesis induced by ROS deletion or pharmacological inhibition of SP1. The data are presented as the means ± standard deviations (SDs). * $p < 0.05$; ** $p < 0.01$; and *** $p < 0.001$

of this combination therapy, especially in the IR + si-PRDM10-DT group ($p < 0.01$). Additionally, the Ki-67 level in IR + si-PRDM10-DT and IR + si-SP1 groups was obviously decreased, indicating that suppression of PRDM10-DT and SP1 can assist the tumor growth inhibition effect of X-ray radiation ($p < 0.01$). Interestingly, the IR or si-PRDM10-DT treatment had no significant effect on SP1 expression, but the silencing of SP1 reduced the increased angiogenesis level induced by IR ($p < 0.001$). Finally, we concluded that the removal of PRDM10-DT or SP1 in tumor tissues can significantly inhibit tumor angiogenesis during radiotherapy. However, much more research is needed to fully investigate the potential of PRDM10-DT and SP1 as molecular targets for inhibiting tumor angiogenesis in therapeutic photon irradiation.

Discussion

In this study, we investigated the differential epigenetic regulation caused by two types of radiation. On the basis of the RNA-seq and bioinformatics analyses, we concluded that TGF-β1 was involved in PRDM10-DT-induced angiogenesis. TGF-β1 reportedly promotes the expression of VEGF, which acts as a crucial mediator of tumor angiogenesis and regulates the growth of new blood vessels [32, 33, 37]. According to previous findings, through controlling TGF-β1 expression, miR-663a has the ability to delay tumor growth [38]. Therefore, we propose that PRDM10-DT inhibits the competitive binding of miR-663a to TGF-β1 and further enhances VEGF expression by sponging miR-663a. Our research indicated that PRDM10-DT binds to miR-663a and forms a ceRNA regulatory network with TGF-β1 mRNA. Upon stimulation with photon irradiation, but not with carbon ion irradiation, the SP1/PRDM10-DT/TGF-β1 axis regulates tumor angiogenesis and metastasis by targeting VEGF (Fig. 7).

Research has confirmed several radiation-induced angiogenic factors, including ErbB, IGF-1, EGFR, PI3K, MAPK, c-Jun N, p38MAP, Fas-R, TNF-R, and NF-κB [39]. These factors can target VEGF or HIF-1α directly or indirectly [40]. The known angiogenic pathway responding to radiation include COX-2/PGH2/TXA2, COX-2/PGE2/HIF-1α/VEGF, NOS/PI3K/Akt/FRAP, NOS/PI3K/Akt/mTOR, EGFR/Ras/MEK/MAPK, EGFR/Ras/MEK/ERK/MNK, EGFR/PI3K/Akt/FRAP [41–45]. These studies revealed that radiation stimulates angiogenesis through multiple molecular pathways, most of which involve the activation of HIF-1α/VEGF. Besides, extracellular vesicles also play an important role in radiation-induced tumor angiogenesis in some tumors [46]. By comparison, our research revealed a novel radiation-responsive angiogenesis regulation axis, i.e., SP1/PRDM10-DT/TGF-β1, which also culminates in enhanced VEGF signaling (Fig. 7). However, the pro-angiogenesis function of PRDM10-DT and its radiation responsiveness has not been reported before, especially its differential response to X-ray and C-ion radiation. This identified pathway supplied a new target for antiangiogenic therapy, especially for photon radiation combined tumor antiangiogenic therapy.

Importantly, serum concentrations of TGF-β1 and VEGF were found to be significantly up-regulated in patients receiving X-ray radiotherapy but not C-ion radiotherapy, a result consistent with many clinical studies. For example, Zhao et al. reported that in lung cancer patients, serum TGF-β1 was significantly increased after receiving radiotherapy and its level was strongly correlated with the severity of radiotherapy-induced radiopulmonary toxicity [47]. Besides, radiation exposure leads to the generation of large amounts of ROS, which not only directly damage tumor cells, but also further upregulate the expression of angiogenic factors, such as VEGF, by activating transcription factors, such as HIF-1α [48]. These angiogenic factors support tumor growth and metastasis by promoting endothelial cell proliferation, migration, and vascular permeability, enhancing tumor vascularization. ROS further enhanced the expression of angiogenic factors through activation of signaling pathways, such as MAPK and NF-κB, thus promoting angiogenesis [49, 50].

In this work, we found a novel role that the ROS-responsive transcription factor SP1 participates in the regulation of angiogenesis by promoting the transcription of PRDM10-DT in NSCLC. The removal of ROS or suppression of SP1 reduced the transcription of PRDM10-DT and hampered the capacity of the cells to

(See figure on next page.)

Fig. 6 Silencing of PRDM10-DT or SP1 can decrease X-ray-induced tumor angiogenesis in vivo. **A** Graphical illustration of the subcutaneous A549 tumor model (SC injection), X-ray irradiation, and drug treatment (created with BioRender.com). **B** Photograph of dissected tumors described in **A**. **C** Subcutaneous tumor growth curve after 40 days of treatment. $n = 5$. **D** The weights of the dissected tumors were measured as described in **A**. $n = 5$. **E** The levels of TGF-β1 and VEGF in the serum of the mice described in **A** were tested via ELISA. $n = 5$. **F** The dissected tumor tissues were processed into sections and then subjected to H&E or IHC staining. The graphs of these sections were taken via the DMS-10 Digital Pathological Section Scanner System. Scale bar = 50 μm. The results of the IHC quantification of CD31, Ki67, VEGF, TGF-β1, and SP1 expression and the MVD of the dissected tumor tissues were analyzed with ImageJ software. The yellow dotted line indicates microvessels in the tumor sections. $n = 5$. The data are presented as the means ± standard deviations (SDs). ^{ns} $p > 0.05$; * $p < 0.05$; ** $p < 0.01$; and *** $p < 0.001$

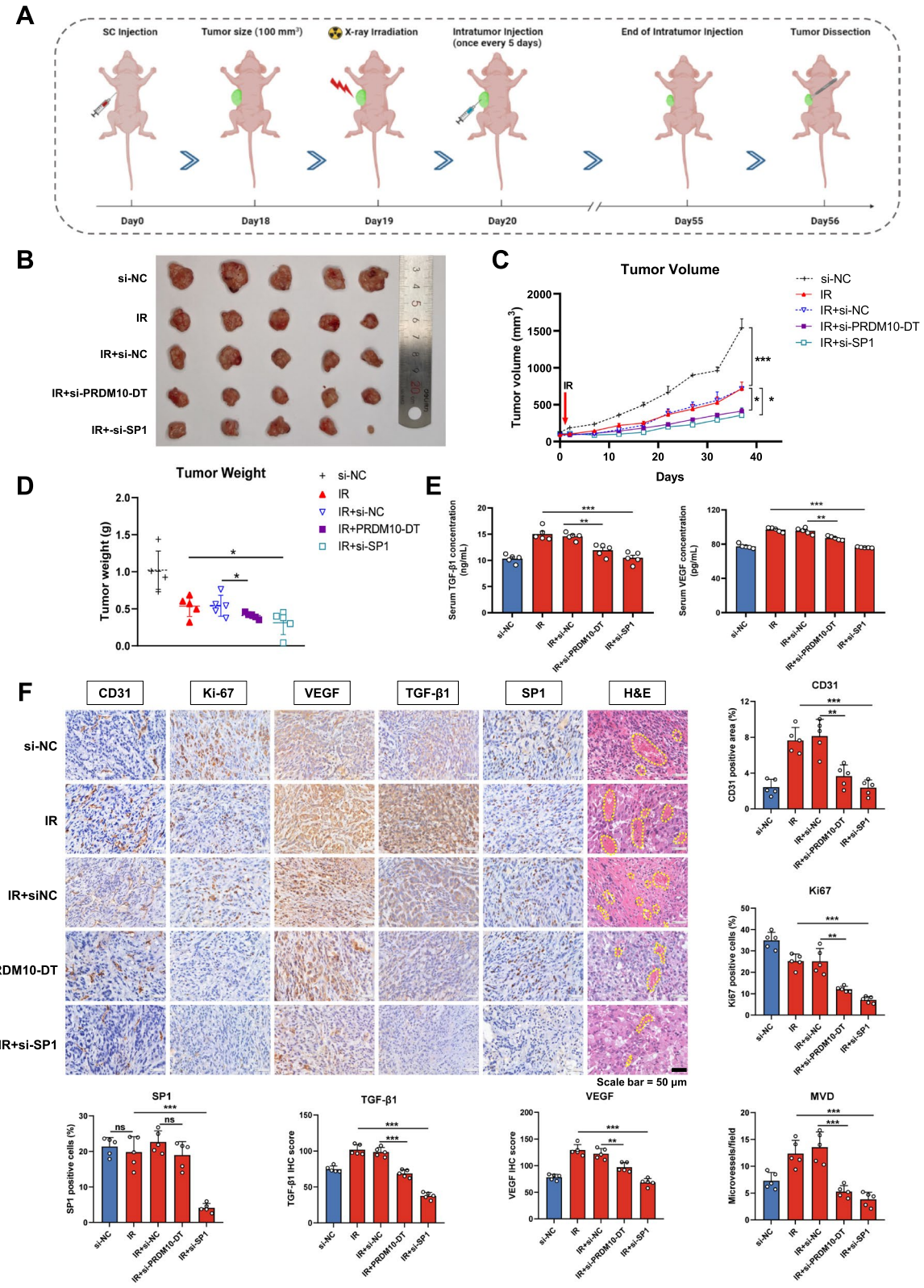

Fig. 6 (See legend on previous page.)

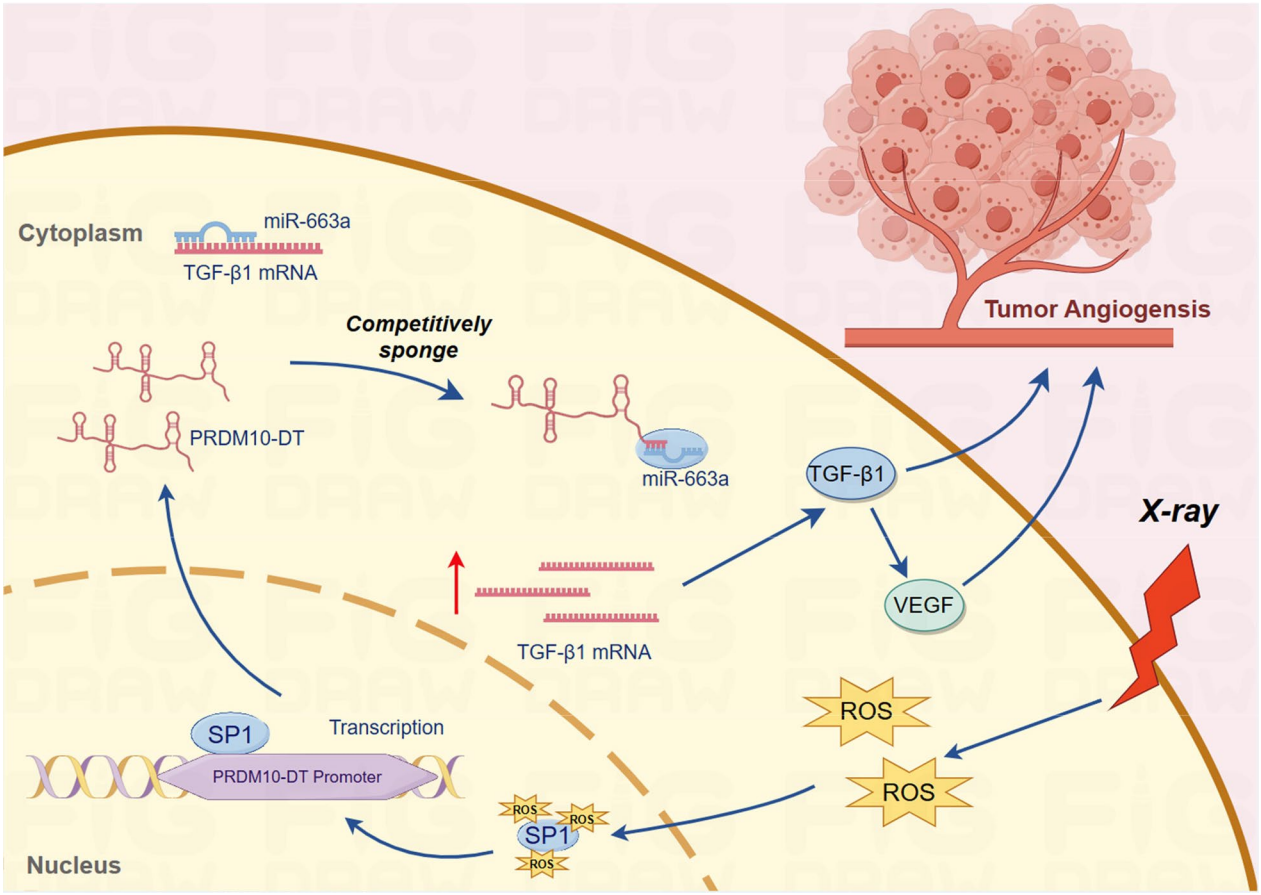

Fig. 7 Mechanistic model of X-ray irradiation-induced tumor angiogenesis through PRDM10-DT/miR-663a/TGF-β1 axis that activated by SP1 in lung adenocarcinoma cells. Radiation activates SP1 binding to PRDM10-DT promoter region and enhances the transcription of PRDM10-DT. Up-regulated PRDM10-DT competitively binds miR-663a and then promotes TGF-β1 and VEGF expression and facilitates tumor angiogenesis

undergo angiogenesis and metastasize. SP1 has been reported to participate in angiogenesis regulating, and low-dose laser radiation can stimulate the transactivation and DNA-binding properties of SP1 on the VEGF promoter [51, 52]. These studies revealed a close relationship between SP1 and angiogenesis. However, the connection between SP1 and radiation-induced angiogenesis in radiotherapy, as well as the varying response of SP1 to radiations of varying quality, is the subject of relatively few studies. Our research shows how SP1 causes a distinct angiogenic response when cells are exposed to photon and heavy ion radiation.

This study was limited by the lack of direct clinical data from patients regarding PRDM10-DT expression because the clinical samples are difficult to acquire from the Department of Radiation Oncology. Although we used a variety of in vitro and in vivo models to investigate potential mechanisms, these models may not fully capture the complex dynamics of human tumor biology. Another potential limitation is the use of a relatively limited range of experimental conditions, which may not include all radiation doses, schedules, or tumor microenvironments observed in clinical practice. In addition, the reliance on specific biomarkers (e.g., VEGF and TGF-β1) may overlook other key pathways or molecules involved in radiation-induced angiogenesis and metastasis. For example, the immune escape effect of the tumor microenvironment and related markers (e.g., PD-L1) are closely associated with angiogenesis [25, 53]. In further study, we would pay more attention to the complex interactions between immune cells, immune-related factors, and angiogenic factors under radiation.

Translational studies carried out in clinical laboratories must be better integrated with basic research aiming at resolving clinical concerns [54, 55]. In future studies, by treating cells and cancer animals with combinations of radiation and specific inhibitors of PRDM10-DT or SP1, we will conduct mechanistic studies and evaluate the safety, efficacy, and biomarker-driven therapeutic strategies of the combination

therapy with radiotherapy and PRDM10-DT or SP1 inhibitors, and explore the possible combination therapies with immunotherapy in order to provide additional benefits, enhance anti-tumor immune responses and the effects on the tumor vascular system. These studies may ultimately lead to more personalized and effective treatments for cancer patients receiving radiotherapy.

Conclusions

In summary, our research revealed that PRDM10-DT functions in an SP1-dependent manner in tumor angiogenesis and metastasis caused by irradiation. By preventing tumor angiogenesis and metastasis, suppressing the SP1/PRDM10-DT/TGF-β1 axis may be a supplementary tactic for conventional photon radiation therapy.

Supplementary Information

The online version contains supplementary material available at https://doi.org/10.1186/s12967-025-06273-0.

Additional file 1.

Acknowledgements

We appreciate the kind giving of patients' serum samples by Prof. Lin Kong in the Shanghai Proton and Heavy Ion Hospital. We are also grateful to the Accelerator staff of HIMAC for their hard work in providing the carbon beams.

Author contributions

H. Huang, W. Hu, T.K. Hei, and G. Zhou developed the concept of this work, designed the experiment project, and wrote the manuscript. H. Huang, Y. Xu, M. Zhang, J. Nie, and Z. Guo operated the molecular and biological experiments. H. Huang, W. Li, and Y. Song performed the bioinformatic analysis of the RNA-seq results. All authors have read and agreed to the published version of the manuscript.

Funding

This work was supported by the National Natural Science Foundation of China (12475350, 82192883, 32071243), the National Key R&D program of China (2018YFC0115704), Collaborative Innovation Center of Radiological Medicine of Jiangsu Higher Education Institutions, and a project funded by the Priority Academic Program Development of Jiangsu Higher Education Institutions (PAPD).

Availability of data and materials

All data generated or analyzed during this work are included in this article and its Additional files.

Declarations

Ethics approval and consent to participate

This work was approved by the Institutional Animal Care and Use Committee of Soochow University.

Consent for publication

All authors have agreed with the publication of this manuscript.

Competing interests

The authors declared there are no conflicts of competing interests in this work.

Author details

[1]State Key Laboratory of Radiation Medicine and Protection, School of Radiation Medicine and Protection, Collaborative Innovation Center of Radiological Medicine of Jiangsu Higher Education Institutions, Soochow University, Suzhou 215123, China. [2]School of Biology and Basic Medical Sciences, Soochow University, Suzhou 215123, China. [3]Center for Radiological Research, College of Physician and Surgeons, Columbia University, New York, NY 10032, USA.

Received: 26 September 2024 Accepted: 18 February 2025
Published online: 27 February 2025

References

1. Bray F, et al. Global cancer statistics 2022: GLOBOCAN estimates of incidence and mortality worldwide for 36 cancers in 185 countries. CA Cancer J Clin. 2024;74:229–63. https://doi.org/10.3322/caac.21834.
2. Abdel-Wahab M, et al. Global radiotherapy: current status and future directions-white paper. JCO Glob Oncol. 2021;7:827–42. https://doi.org/10.1200/GO.21.00029.
3. Kim E, et al. Clinical utilization of radiation therapy in Korea, 2016. J Radiat Res. 2020;61:249–56. https://doi.org/10.1093/jrr/rrz095.
4. Datta NR, Rogers S, Bodis S. Challenges and opportunities to realize "the 2030 agenda for sustainable development" by the United Nations: implications for radiation therapy infrastructure in low- and middle-income countries. Int J Radiat Oncol Biol Phys. 2019;105:918–33. https://doi.org/10.1016/j.ijrobp.2019.04.033.
5. Zheng M, Liu Z, He Y. Radiation-induced fibrosis: mechanisms and therapeutic strategies from an immune microenvironment perspective. Immunology. 2024;172:533–46. https://doi.org/10.1111/imm.13788.
6. Najafi M, et al. Mechanisms of inflammatory responses to radiation and normal tissues toxicity: clinical implications. Int J Radiat Biol. 2018;94:335–56. https://doi.org/10.1080/09553002.2018.1440092.
7. Gandhi S, Chandna S. Radiation-induced inflammatory cascade and its reverberating crosstalks as potential cause of post-radiotherapy second malignancies. Cancer Metastasis Rev. 2017;36:375–93. https://doi.org/10.1007/s10555-017-9669-x.
8. Atajanova T, Rahman MM, Konieczkowski DJ, Morris ZS. Radiation-associated secondary malignancies: a novel opportunity for applying immunotherapies. Cancer Immunol Immunother. 2023;72:3445–52. https://doi.org/10.1007/s00262-023-03532-1.
9. Triner D, Shah YM. Hypoxia-inducible factors: a central link between inflammation and cancer. J Clin Invest. 2016;126:3689–98. https://doi.org/10.1172/JCI84430.
10. Aghapour SA, et al. Investigating the dynamic interplay between cellular immunity and tumor cells in the fight against cancer: an updated comprehensive review. Iran J Blood Cancer. 2024;16:84–101. https://doi.org/10.61186/ijbc.16.2.84
11. Aghaei M, et al. Genetic variants of dectin-1 and their antifungal immunity impact in hematologic malignancies: a comprehensive systematic review. Curr Res Transl Med. 2024;72: 103460. https://doi.org/10.1016/j.retram.2024.103460.
12. O'Malley J, et al. Radiation therapy-induced metastasis and secondary malignancy. In: Encyclopedia of Cancer. 3rd ed. Elsevier; 2019. pp. 337-46. https://doi.org/10.1016/B978-0-12-801238-3.65171-1.
13. Kamada T, et al. Carbon ion radiotherapy in Japan: an assessment of 20 years of clinical experience. Lancet Oncol. 2015;16:e93–100. https://doi.org/10.1016/S1470-2045(14)70412-7.
14. Li Y, et al. Flourish of proton and carbon ion radiotherapy in China. Front Oncol. 2022;12: 819905. https://doi.org/10.3389/fonc.2022.819905.
15. Nakajima K, et al. Clinical outcomes of image-guided proton therapy for histologically confirmed stage I non-small cell lung cancer. Radiat Oncol. 2018;13:199. https://doi.org/10.1186/s13014-018-1144-5.
16. Kamlah F, et al. Comparison of the effects of carbon ion and photon irradiation on the angiogenic response in human lung adenocarcinoma cells. Int J Radiat Oncol Biol Phys. 2011;80:1541–9. https://doi.org/10.1016/j.ijrobp.2011.03.033.
17. Tinganelli W, Durante M. Carbon ion radiobiology. Cancers. 2020;12:3022. https://doi.org/10.3390/cancers12103022.

18. Chen Y, Li Z, Chen X, Zhang S. Long non-coding RNAs: from disease code to drug role. Acta Pharm Sin B. 2021;11:340–54. https://doi.org/10.1016/j.apsb.2020.10.001.
19. Ponnusamy M, et al. Long noncoding RNA CPR (cardiomyocyte proliferation regulator) regulates cardiomyocyte proliferation and cardiac repair. Circulation. 2019;139:2668–84. https://doi.org/10.1161/CIRCULATIONAHA.118.035832.
20. Reuter S, Gupta SC, Chaturvedi MM, Aggarwal BB. Oxidative stress, inflammation, and cancer: how are they linked? Free Radic Biol Med. 2010;49:1603–16. https://doi.org/10.1016/j.freeradbiomed.2010.09.006.
21. Matsumoto K-I, Nyui M, Ueno M, Ogawa Y, Nakanishi I. A quantitative analysis of carbon-ion beam-induced reactive oxygen species and redox reactions. J Clin Biochem Nutr. 2019;65:1–7. https://doi.org/10.3164/jcbn.18-34.
22. Hu W, et al. Overexpression of Ras-related C3 botulinum toxin substrate 2 radiosensitizes melanoma cells in vitro and in vivo. Oxid Med Cell Longev. 2019;2019:5254798. https://doi.org/10.1155/2019/5254798.
23. Lau BC, et al. Pulmonary hemorrhage in patients treated with thoracic stereotactic ablative radiotherapy and antiangiogenic agents. J Thorac Oncol. 2023;18:922–30. https://doi.org/10.1016/j.jtho.2023.04.007.
24. Neves KB, Montezano AC, Lang NN, Touyz RM. Vascular toxicity associated with anti-angiogenic drugs. Clin Sci. 2020;134:2503–20. https://doi.org/10.1042/CS20200308.
25. Lee WS, Yang H, Chon HJ, Kim C. Combination of anti-angiogenic therapy and immune checkpoint blockade normalizes vascular-immune crosstalk to potentiate cancer immunity. Exp Mol Med. 2020;52:1475–85. https://doi.org/10.1038/s12276-020-00500-y.
26. Park H, Nam KS, Lee HJ, Kim KS. Ionizing radiation-induced GDF15 promotes angiogenesis in human glioblastoma models by promoting VEGFA expression through p-MAPK1/SP1 signaling. Front Oncol. 2022;12:801230. https://doi.org/10.3389/fonc.2022.801230.
27. Yamada S, et al. Carbon-ion radiotherapy for colorectal cancer. J Anus Rectum Colon. 2021;5:113–20. https://doi.org/10.23922/jarc.2020-082.
28. Matsumoto Y, et al. Antimetastatic effects of carbon-ion beams on malignant melanomas. Radiat Res. 2018;190:412–23. https://doi.org/10.1667/RR15075.1.
29. Weis SM, Cheresh DA. Tumor angiogenesis: molecular pathways and therapeutic targets. Nat Med. 2011;17:1359–70. https://doi.org/10.1038/nm.2537.
30. Altorki NK, et al. The lung microenvironment: an important regulator of tumour growth and metastasis. Nat Rev Cancer. 2019;19:9–31. https://doi.org/10.1038/s41568-018-0081-9.
31. Ando T, et al. Tumor-specific interendothelial adhesion mediated by FLRT2 facilitates cancer aggressiveness. J Clin Invest. 2022;132: e153626. https://doi.org/10.1172/JCI153626.
32. Chen Y, et al. TGFβ1 as a predictive biomarker for collateral formation within ischemic moyamoya disease. Front Neurol. 2022;13: 899470. https://doi.org/10.3389/fneur.2022.899470.
33. Wu D, et al. Involvement of Müller glial autoinduction of TGF-β in diabetic fibrovascular proliferation via glial-mesenchymal transition. Invest Ophthalmol Vis Sci. 2020;61:29. https://doi.org/10.1167/iovs.61.14.29.
34. Matsumoto K-I, Ueno M, Shoji Y, Nakanishi I. Heavy-ion beam-induced reactive oxygen species and redox reactions. Free Radical Res. 2021;55:450–60. https://doi.org/10.1080/10715762.2021.1899171.
35. Ahmad HI, et al. Molecular evolution of the activating transcription factors shapes the adaptive cellular responses to oxidative stress. Oxid Med Cell Longev. 2022;2022:2153996. https://doi.org/10.1155/2022/2153996.
36. Aggarwal V, et al. Role of reactive oxygen species in cancer progression: molecular mechanisms and recent advancements. Biomolecules. 2019;9:735. https://doi.org/10.3390/biom9110735.
37. Zheng W, Seftor EA, Meininger CJ, Hendrix MJ, Tomanek RJ. Mechanisms of coronary angiogenesis inresponse to stretch: role of VEGF and TGF-beta. Am J Physiol Heart Circ Physiol. 2001;280:H909–17. https://doi.org/10.1152/ajpheart.2001.280.2.H909
38. Zhang C, et al. miR-663a inhibits tumor growth and invasion by regulating TGF-β1 in hepatocellular carcinoma. BMC Cancer. 2018;18:1179. https://doi.org/10.1186/s12885-018-5016-z.
39. Sorolla MA, Parisi E, Sorolla A. Determinants of sensitivity to radiotherapy in endometrial cancer. Cancers. 2020;12:1906. https://doi.org/10.3390/cancers12071906.
40. Banys-Paluchowski M, et al. The clinical relevance of serum vascular endothelial growth factor (VEGF) in correlation to circulating tumor cells and other serum biomarkers in patients with metastatic breast cancer. Breast Cancer Res Treat. 2018;172:93–104. https://doi.org/10.1007/s10549-018-4882-z.
41. Anoopkumar-Dukie S, et al. The COX-2 inhibitor NS398 selectively sensitizes hypoxic HeLa cells to ionising radiation by mechanisms both dependent and independent of COX-2. Prostaglandins Other Lipid Mediat. 2020;148: 106422. https://doi.org/10.1016/j.prostaglandins.2020.106422.
42. Mitryayeva NA, Grebinyk LV, Uzlenkova NE. Influence of combined action of X-radiation and cyclooxygenase-2—meloxivet inhibitor on VEGF AND PGE-2 content in blood of rat-tumor carriers. Probl Radiac Med Radiobiol. 2019;24:261–9. https://doi.org/10.33145/2304-8336-2019-24-261-269.
43. Li Y, Sun R, Zou J, Ying Y, Luo Z. Dual roles of the AMP-activated protein kinase pathway in angiogenesis. Cells. 2019;8:752. https://doi.org/10.3390/cells8070752.
44. Holotiuk VV, Kryzhanivska AY, Churpiy IK, Tataryn BB, Ivasiutyn DY. Role of nitric oxide in pathogenesis of tumor growth and its possible application in cancer treatment. Exp Oncol. 2019;41:210–5. https://doi.org/10.32471/exp-oncology.2312-8852.vol-41-no-3.13515.
45. Alique M, et al. Hypoxia-inducible factor-1α: the master regulator of endothelial cell senescence in vascular aging. Cells. 2020;9:195. https://doi.org/10.3390/cells9010195.
46. Zheng Y, et al. The extracellular vesicles secreted by lung cancer cells in radiation therapy promote endothelial cell angiogenesis by transferring miR-23a. PeerJ. 2017;5: e3627. https://doi.org/10.7717/peerj.3627.
47. Zhao L, et al. Elevation of plasma TGF-beta1 during radiation therapy predicts radiation-induced lung toxicity in patients with non-small-cell lung cancer: a combined analysis from Beijing and Michigan. Int J Radiat Oncol Biol Phys. 2009;74:1385–90. https://doi.org/10.1016/j.ijrobp.2008.10.065.
48. Wei J, et al. Radiation-induced normal tissue damage: oxidative stress and epigenetic mechanisms. Oxid Med Cell Longev. 2019;2019:3010342. https://doi.org/10.1155/2019/3010342.
49. Shi X, Li M, Huang Q, Xie L, Huang Z. Monacolin K induces apoptosis of human glioma U251 cells by triggering ROS-mediated oxidative damage and regulating MAPKs and NF-κB pathways. ACS Chem Neurosci. 2023;14:1331–41. https://doi.org/10.1021/acschemneuro.3c00104.
50. Lian S, Li S, Zhu J, Xia Y, Do Jung Y. Nicotine stimulates IL-8 expression via ROS/NF-κB and ROS/MAPK/AP-1 axis in human gastric cancer cells. Toxicology. 2022;466: 153062. https://doi.org/10.1016/j.tox.2021.153062.
51. Xu K, Gao H, Shu H-KG. Celecoxib can induce vascular endothelial growth factor expression and tumor angiogenesis. Mol Cancer Ther. 2011;10:138–47. https://doi.org/10.1158/1535-7163.MCT-10-0415.
52. Feng J, Zhang Y, Xing D. Low-power laser irradiation (LPLI) promotes VEGF expression and vascular endothelial cell proliferation through the activation of ERK/Sp1 pathway. Cell Signal. 2012;24:1116–25. https://doi.org/10.1016/j.cellsig.2012.01.013.
53. Yu J, et al. Nuclear PD-L1 promotes EGR1-mediated angiogenesis and accelerates tumorigenesis. Cell Discov. 2023;9:33. https://doi.org/10.1038/s41421-023-00521-7.
54. Aghaei M, Khademi R, Bahreiny SS, Saki N. The need to establish and recognize the field of clinical laboratory science (CLS) as an essential field in advancing clinical goals. Health Sci Rep. 2024;7: e70008. https://doi.org/10.1002/hsr2.70008.
55. Saki N, Haybar H, Aghaei M. Subject: motivation can be suppressed, but scientific ability cannot and should not be ignored. J Transl Med. 2023;21:520. https://doi.org/10.1186/s12967-023-04383-1.

Publisher's Note